Supporting information for

Dual impact of water on stability of metal-organic frameworks

Fatemeh Keshavarz*

Department of Physics, School of Engineering Science, LUT University,
Yliopistonkatu 34, FI-53850 Lappeenranta, Finland.

*Corresponding author: fatemeh.keshavarz@lut.fi

Section S1. Computational details

To study the interactions and reactions of water with the MOFs, both periodic and fragment/model-based simulations were performed. For periodic simulations, the unit cells of HKUST-1,[1] MOF-303,[2] and UMCM-1[3] were retrieved from the Cambridge Structural Database (CSD)[4] using 2091245, 2078717, and 668919 accession codes, respectively. In the reported crystal structure of UMCM-1, there were some ligands with mirror reflections and partial atomic occupancies. Because of the incapability of the simulation program in addressing partial occupancies, the reflected ligand atoms were removed manually, and the occupancies of the conserved atoms were set to unity. No crystal structure was reported for MIL-127(Fe). Therefore, the unit cell structure of MIL-127(Al) (CSD code: 1510859)[5] was adopted, and its Al atoms were replaced with Fe. Then, the fragmented models were generated by extracting the main metal node and its fully extended ligands from the unit cell structures. The free connectivity points, such as the free oxygen atoms in the carboxylate groups, were capped by hydrogen. The resultant models are shown in Fig. 1 of the main text.

All simulated models were considered in their ground spin state. According to our previous study on various MOF models,[6] the MOF-303 (Al^{3+}) and UMCM-1 (Zn^{2+}) unit cells and cluster models were studied in their singlet spin state as neutral structures. However, all Fe^{3+} atoms of MIL-127 were considered in their highest spin state, and the metal node was evaluated as a non-neutral structure based on its connectivity pattern and composition. Therefore, the fragmented MIL-127 (Fe) model was simulated as a 16tet structure with +1 charge. For HKUST-1, our previous study[6] had shown that the Cu^{2+} atoms of paddlewheel structures can assume different spin states with paired and unpaired electrons. Therefore, both singlet and triplet spin states were evaluated for the HKUST-1 model, which was considered as a charge neutral structure.

S1.1 Periodic simulations

Water interactions with periodic MOF structures were studied using periodic density functional theory (DFT) simulations by Vienna Ab Initio Simulation Package (VASP)[7,8] v. 6.3.0. The water-free unit cells of HKUST-1, MIL-127(Fe), MOF-303, and UMCM-1 contained 624, 416, 128, 510 atoms, respectively. With axial water molecules, the HKUST-1 and MIL-127(Fe) respectively contained 768 and 488 atoms. We placed the guest water molecule in the center of their pores and permitted the water to relax in the most stable adsorption site. For structures with large pores, like UMCM-1, we also positioned a guest water molecule near their metal

node. All periodic structures were treated similarly using a cut-off energy of 450 eV and Γ-point sampling of the Brillouin zone through a 1 × 1 × 1 Monkhorst-Pack grid. The inter-atomic interactions were evaluated using the strongly constrained and appropriately normed (SCAN) functional,[9] which is a meta-generalized gradient approximation (meta-GGA) method with superior performance relative to most gradient-corrected functionals.[10] Along with the SCAN functional, projector augmented wave (PAW) pseudopotentials were used.[11] The POTCAR library of VASP was employed to assign the Al (s^2p^1), Cu (d^{10} p^1), Fe (d^7 s^1), Zn (d^{10} p^2), O (s^2p^4), N (s^2p^3), C (s^2p^2), and H (ultrasoft) PAW parameters to the systems. The long-range dispersion effects were included by introducing the DFT-D3 van der Waals corrections with Becke-Jonson damping.[12,13]

The systems were fully optimized by allowing relaxation of all structural parameters including atomic positions, cell shape and cell volume. During the optimization process, spin polarization, the "accurate" precision mode, and the very fast electronic minimization algorithm were used. The convergence criteria included the energy differences of 1×10^{-5} eV and 1×10^{-4} eV for the self-consistent electronic structure calculations, and the ionic relaxation loop, respectively. The conjugate gradient algorithm[14] was used to move and relax the atoms until the force on each atom was below 0.05 eV $Å^{-1}$.

We initially performed the periodic calculations using a 600 eV cutoff and fixed spin states. However, due to very slow electronic convergence for several systems, we reduced the cutoff to 450 eV and lifted the spin constraints. The accuracy of the chosen parameter sets was confirmed by comparing the optimized periodic systems with their experimentally determined crystallographic structures.[1,2] For HKUST-1 (with its axial water molecules) and MOF-303, the root-mean-square-deviations (RMSDs) of 0.398 Å and 0.209 Å were obtained, respectively, confirming acceptability of the applied parameters. For UMCM-1 and MIL-127(Fe), no reliable crystallographic structure was available for comparison. Further, a sensitivity test was carried out for HKUST-1 and MOF-303 by fully optimizing their structures using both 450 eV and 600 eV cutoff. The results showed only minor structural differences caused by the reduction of energy cutoff and lifting the spin constraints (for example, the Cu–Cu distance in HKUST-1 changed by ≤0.016 Å) although the total energies shifted by 32.4 kJ mol^{-1} for MOF-303 and 55.3 kJ mol^{-1} for the water-free triplet HKUST-1. These energy shifts are expected to partially cancel in relative quantities such as adsorption energies. To confirm the expectation, we performed a series of single-point energy calculations using an energy cutoff of 600 and the MIL-127(Fe) and MOF-303 structures optimized at the 450 eV cutoff level (Γ-point only).

The results indicated -0.8 kJ mol^{-1} and -0.9 kJ mol^{-1} change in the water adsorption energies of MIL-127(Fe) and MOF-303, respectively, approving the cancellation of the energy errors during adsorption energy calculations. We repeated a similar sensitivity test on UMCM-1 (with the largest cell volume) and MOF-303 (as the smallest cell) using 450 eV cutoff and a 2 × 2 × 2 grid. The finer grid resulted in a negligible change in the water adsorption energy of UMCM-1 (0.3 kJ mol^{-1}) and a moderate change for MOF-303 (10.9 kJ mol^{-1}). Though these results might alter slightly after full optimization of the structures, they imply an adsorption energy error of maximum ≈10 kJ mol^{-1} for our Γ-point adsorption energy calculations (relative to the finer grid), unaffecting the relative results and qualitative comparisons.

The adopted adjustment substantially improved the convergence behavior though some water-containing periodic models still approached the convergence criteria slowly despite extensive computational effort (>100,000 CPU hours at the 450 eV cutoff). The corresponding structural and energy results were discarded unless they reached the energy convergence criterion of 1×10^{-4} eV (vs. the 1×10^{-5} eV initial criterion). For this reason, the periodic results are used primarily to provide a qualitative picture of the adsorption mechanism, and only those numerical values with acceptable uncertainty are reported.

We also performed periodic molecular dynamics (MD) simulations with rather similar VASP settings. However, as implied by the challenging energy convergences, the size of the systems did not permit the study of the systems over a reasonable time scale. MOF-303 with one guest water molecule was found to be the only system that its dynamics could be simulated for over 0.5 ns with a reasonable computational cost. At the high temperature of 250 °C (at 1 atm), it showed some transient carboxylate ligand detachment. However, the ligand reattached to its metal center fast and the water molecule was not involved in the detachment process. Therefore, the obtained MD results are not reported in this study.

S1.2 Model-based simulations

The fragment-based simulations were performed using the Gaussian 16 C.02 package.[15] As the SCAN functional is not available in Gaussian, the MOF models were optimized using alternative computational levels and the default convergence criteria.[15] The first evaluated level was HSE06/6-31+G* with no additional dispersion correction,[16] which was found to be the optimal level for simulation of many MOF models.[6] This level demonstrated some convergence difficulties because of its highly demanding computations and the large size of the fragmented models. The other evaluated levels included PBE0[17]/LanL2DZ[18,19] and M06-2X[20]/LanL2DZ

with Grimme's dispersion correction (GD3)[12] to account for the long-range van der Waals interactions. The structures optimized at these two levels and their ground spin state were compared with the starting crystallographic structures.[1-3] The comparison by the Chemcraft software[21] indicated that PBE0/LanL2DZ+GD3 gives a lower RMSD (0.9075 Å) relative to M06-2X/LanL2DZ+GD3 (0.9809 Å). Therefore, PBE0/LanL2DZ+GD3 was used for further calculations. Throughout the simulations, harmonic frequency analysis was performed on the optimized structures to distinguish between stable and unstable structures. The structures with no imaginary frequency were deemed as stable structures. Also, we concerned lack of spin contamination for the structures with unpaired electrons.[22,23]

To explore the potential energy surface (PES) of the hydrolysis reactions, the transition states were guessed based on the expected reactions R1 and R2 (see "Introduction" of the main text), earlier experimental[24] or theoretical[25] works on the hydrolysis reaction, intuition, or the quadratic synchronous transit (QST3)[26] transition state allocation approach. All guessed and optimized transition states were checked for imaginary frequencies. If they showed no imaginary frequencies, they were discarded. When an imaginary frequency was observed for a transition state candidate, intrinsic reaction coordinate (IRC) analysis[27,28] was performed to connect it to its associated reactants and products and confirm the reaction path. The corresponding reactants and products were also optimized to confirm their structure and stability and expand the energy surface.

S1.3 Water condensation simulations

The condensation of water inside the MOFs was simulated using the fragmented MOF models and a systematic configurational sampling approach.[6,29] Accordingly, 1, 2, 4, 6, 8, 10, 12 and 16 water molecules were added to the MOF models using the artificial bee colony algorithm of ABCluster 1.4.[30,31] To locate the global minimum (GM) structures in the configurational space, 800 guesses were generated initially and improved by deploying 4 scout bees over 800 cycles. Among the generated water-MOF clusters, 400 structures with the lowest complex formation energies (and highest stability) were given as the local minima (LM) structures. The energies were estimated as the sum of van der Waals and electrostatic interactions. The electrostatic interactions were estimated based on the atomic polar tensor (APT) charges obtained from by the DFT calculations at the PBE0/LanL2DZ+GD3 level. The van der Waals interactions were calculated using the Lennard-Jones parameters taken from the universal force field for MOFs (UFF4MOF).[32] After that, all LM clusters were optimized by the GFN-xTB[33]

semi-empirical method implemented in the XTB 6.0.1[34] program. Then, three of the lowest energy structures presenting structural uniqueness and an energy of no more than 100 kJ mol^{-1} above that of the lowest energy structure were optimized using the PBE0/LanL2DZ+GD3 level method. Finally, the structures giving the lowest Gibbs free energies, at 1 atm and 298.15 K, were selected as the GM structures.

S1.4 Adsorption energy calculations

Regardless of the type of the simulations, the adsorption energies (E_{ad}) for the adsorption of n water molecules were calculated as the difference between the energy of the MOF-water system ($E_{MOF+water}$), the energy of the system in the absence of the guest water molecules (E_{MOF}) and the energy of an isolated water molecule (E_{water}): $E_{ad} = (E_{MOF+water} - E_{MOF} - n\ E_{water})/n$. The corresponding Gibbs energies of adsorption (G_{ad}) at 298.15 K and 1 atm were calculated similarly; $G_{ad} = (G_{MOF+water} - G_{MOF} - n\ G_{water})/n$.

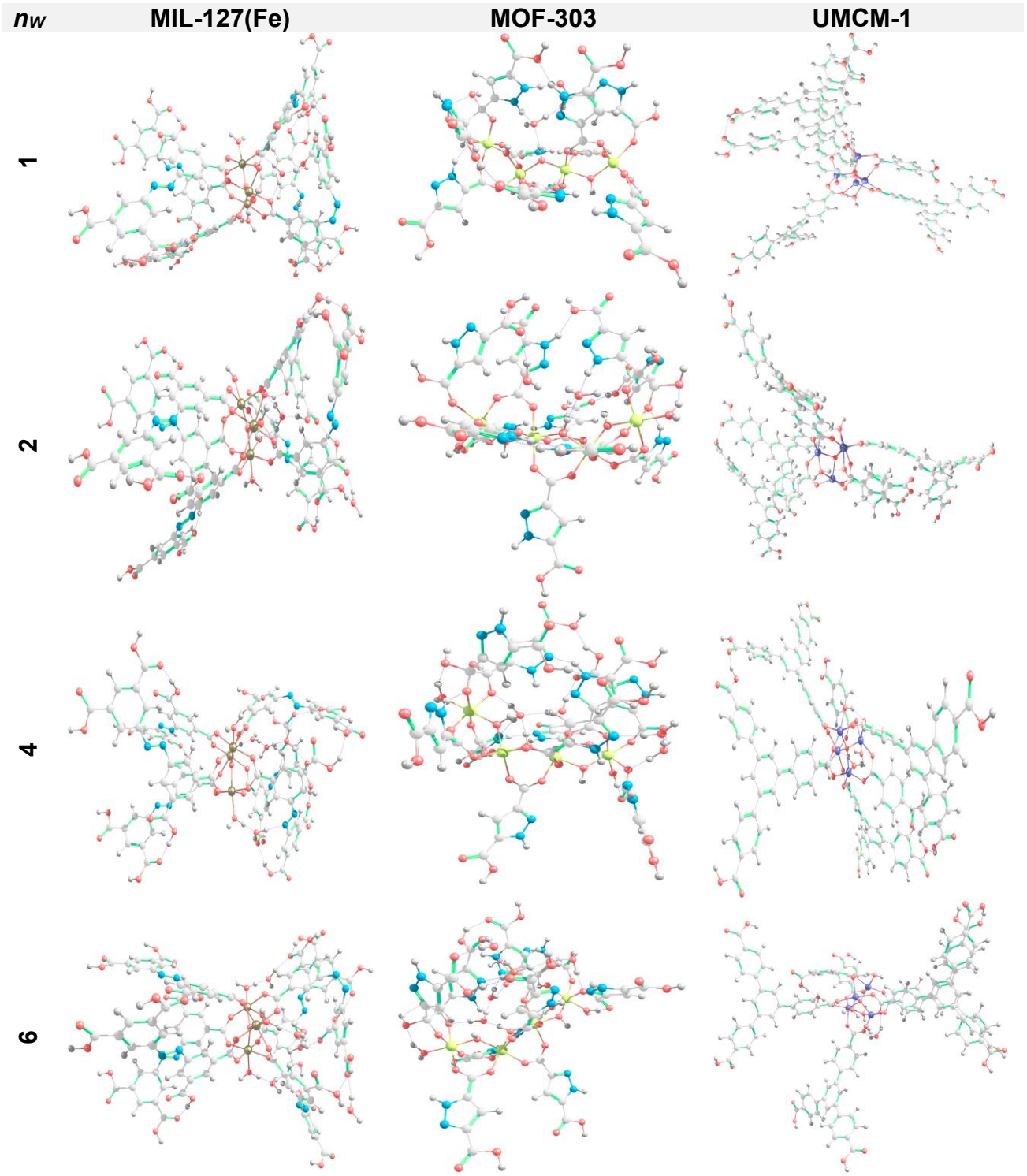
nw
MIL-127(Fe)
MOF-303
UMCM-1
1
2
4
6

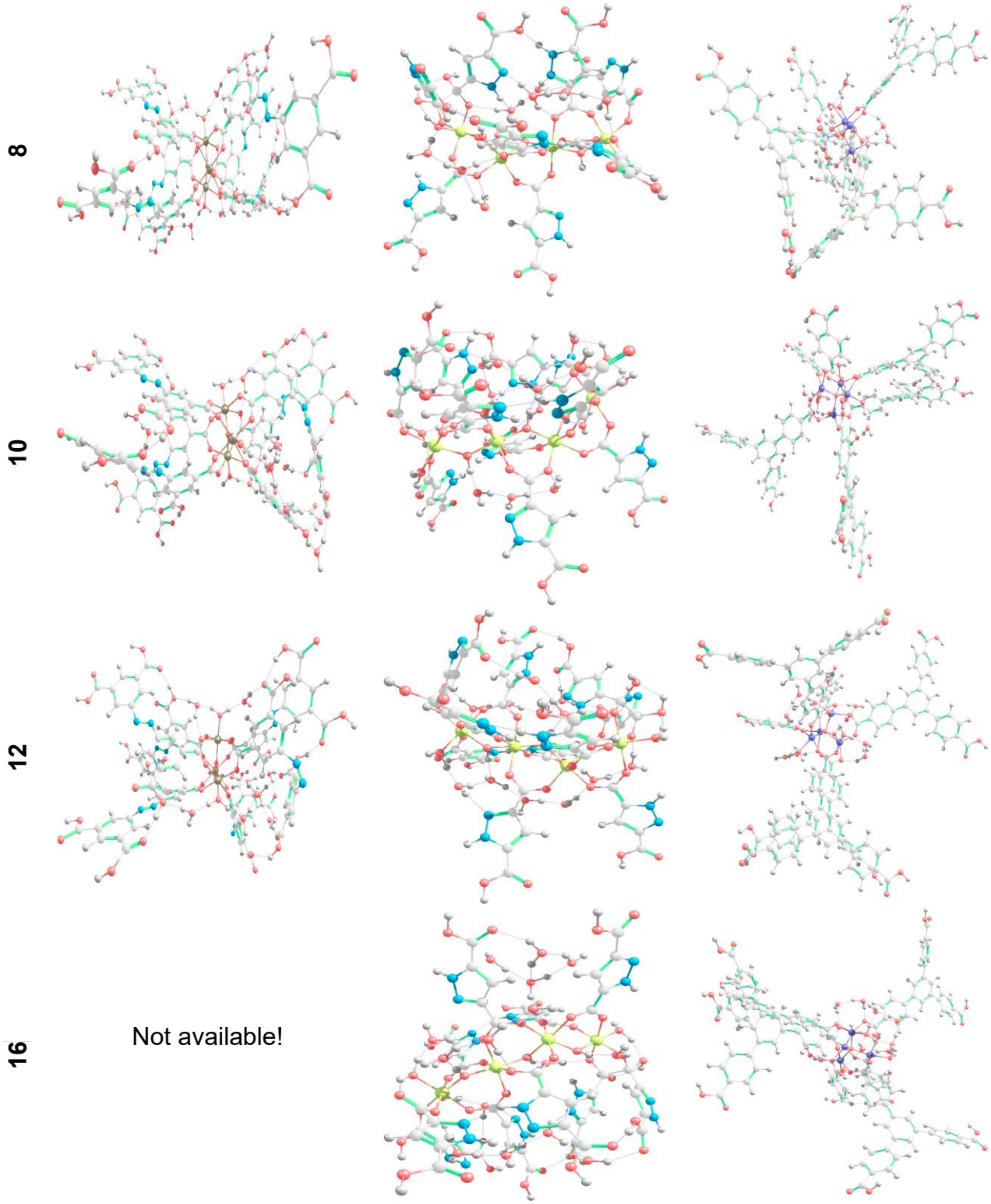

Fig. S1 The adsorption mode of n_W = 1 – 16 water molecules into MIL-127(Fe), MOF-303, and UMCM-1. The Fe, Zn, Al, O, N, C and H atoms are represented by dark yellow, purple, light yellow, red, blue, light grey and white spheres, respectively.

n_W	**HKUST-1** (triplet)	**HKUST-1** (singlet)
1	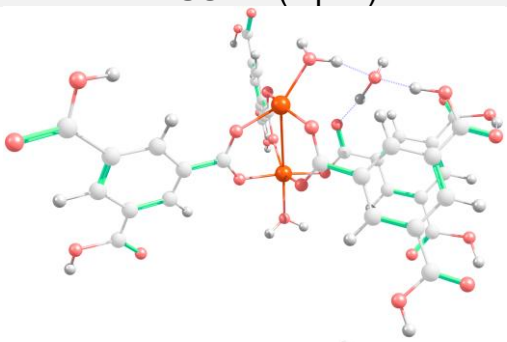	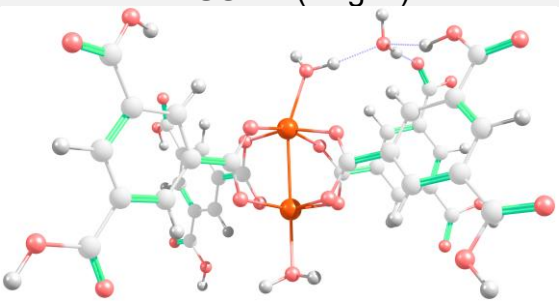
2	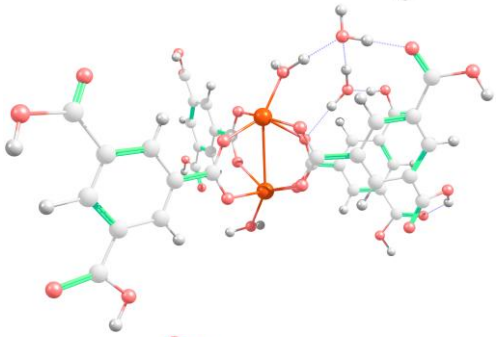	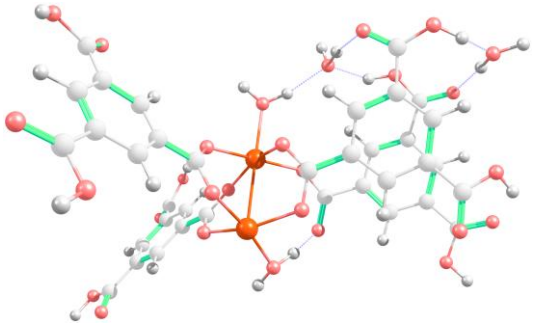
4	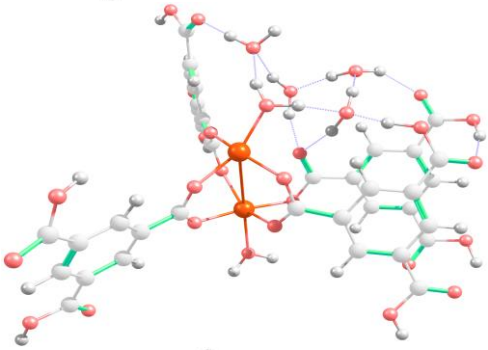	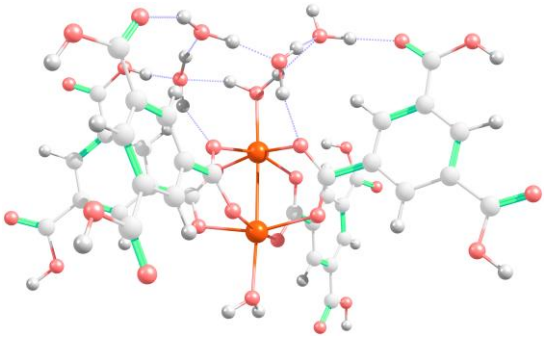
6	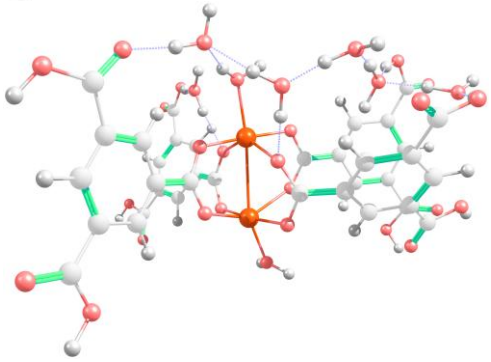	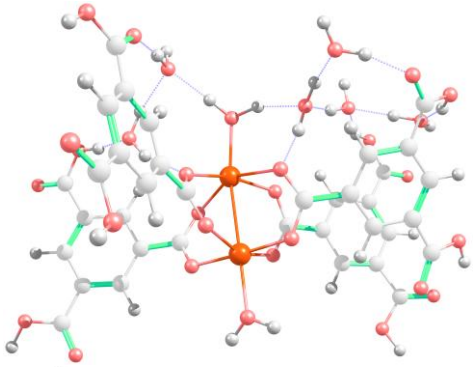
8	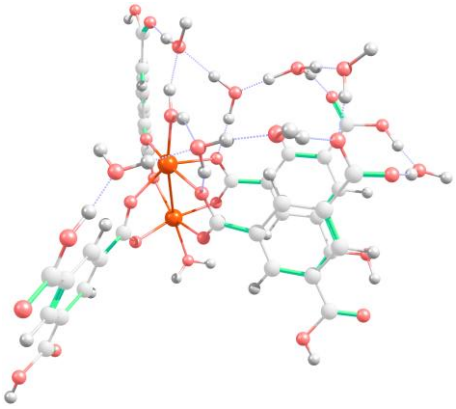	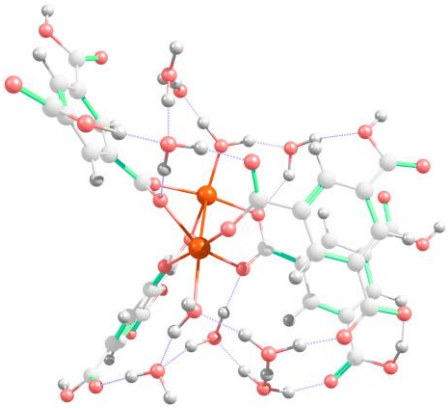

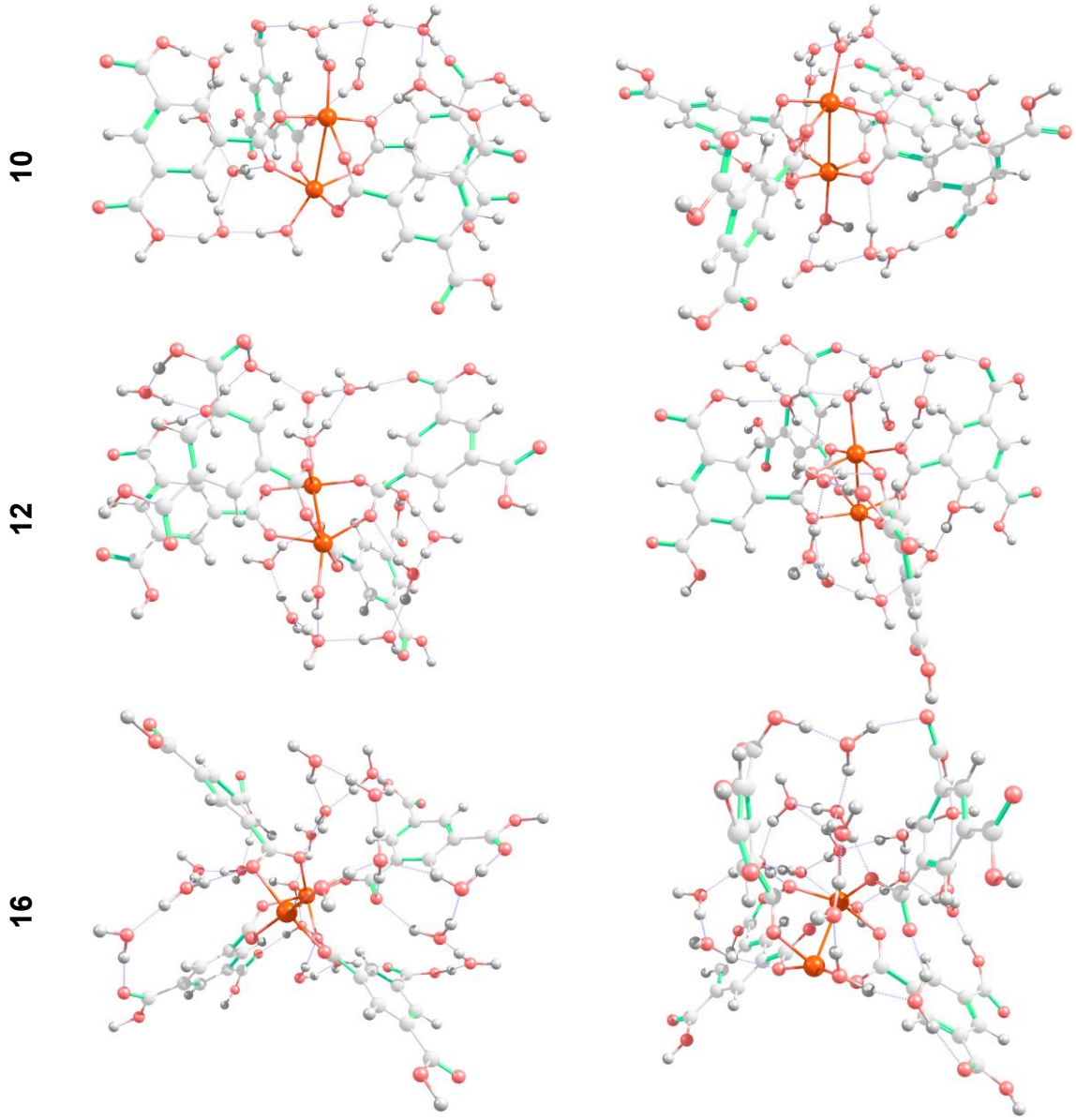

Fig. S2 The adsorption mode of n_W = 1 – 16 water molecules into singlet and triplet HKUST-1. The Cu, O, C and H atoms are represented by orange, red, light grey and white spheres, respectively. The dotted blue lines show hydrogen bonds.

Table S1 The average and stepwise adsorption energies (E_{ad}) and Gibbs free energies (G_{ad}) (kJ mol^{-1}) for the adsorption of n_W = 1 – 16 water molecules.

n_W	HKUST-1 (Singlet)	HKUST-1 (Triplet)	MIL-127	MOF-303	UMCM-1	HKUST-1 (Singlet)	HKUST-1 (Triplet)	MIL-127	MOF-303	UMCM-1
			E_{ad}					G_{ad}		
					Average					
1	-104.1	-156.2	-100.4	-177.2	-177.5	-49.7	-82.0	-31.3	-104.5	-85.5
2	-122.9	-110.3	-115.8	-99.2	-144.3	-65.5	-55.6	-56.9	-54.3	-66.9
4	-95.0	-112.4	-118.8	-120.8	-117.6	-49.4	-61.1	-67.3	-74.9	-59.6
6	-99.8	-95.7	-110.2	-121.1	-101.3	-53.7	-49.6	-62.5	-76.9	-51.1
8	-101.1	-107.6	-104.6	-105.3	-90.6	-54.1	-61.9	-59.1	-61.9	-44.3
10	-93.1	-93.5	-94.6	-105.4	-93.9	-48.5	-48.0	-50.5	-62.6	-49.0
12	-81.8	-90.2	-93.4	-104.7	-90.3	-38.4	-46.5	-48.9	-61.9	-46.4
16	-88.6	-89.5	-	-82.1	-89.1	-45.3	-46.3	-	-40.1	-44.9
					Stepwise					
1	-104.1	-156.2	-100.4	-177.2	-177.5	-49.7	-82.0	-31.3	-104.5	-85.5
2	-141.7	-64.4	-131.3	-21.2	-111.2	-81.4	-29.2	-82.6	-4.1	-48.3
4	-67.1	-114.4	-121.8	-142.4	-90.9	-33.2	-66.5	-77.6	-95.6	-52.2
6	-109.5	-62.3	-93.0	-121.6	-68.6	-62.2	-26.7	-52.9	-80.8	-34.3
8	-104.9	-143.2	-87.8	-57.9	-58.6	-55.6	-99.0	-49.1	-16.8	-23.9
10	-61.0	-37.3	-54.3	-105.9	-107.2	-25.9	+7.9	-16.2	-65.5	-67.7
12	-25.4	-73.9	-87.9	-101.4	-72.3	+12.0	-39.2	-40.7	-58.5	-33.5
16	-109.1	-87.2	-	-14.1	-85.4	-65.9	-45.7	-	25.3	-40.4

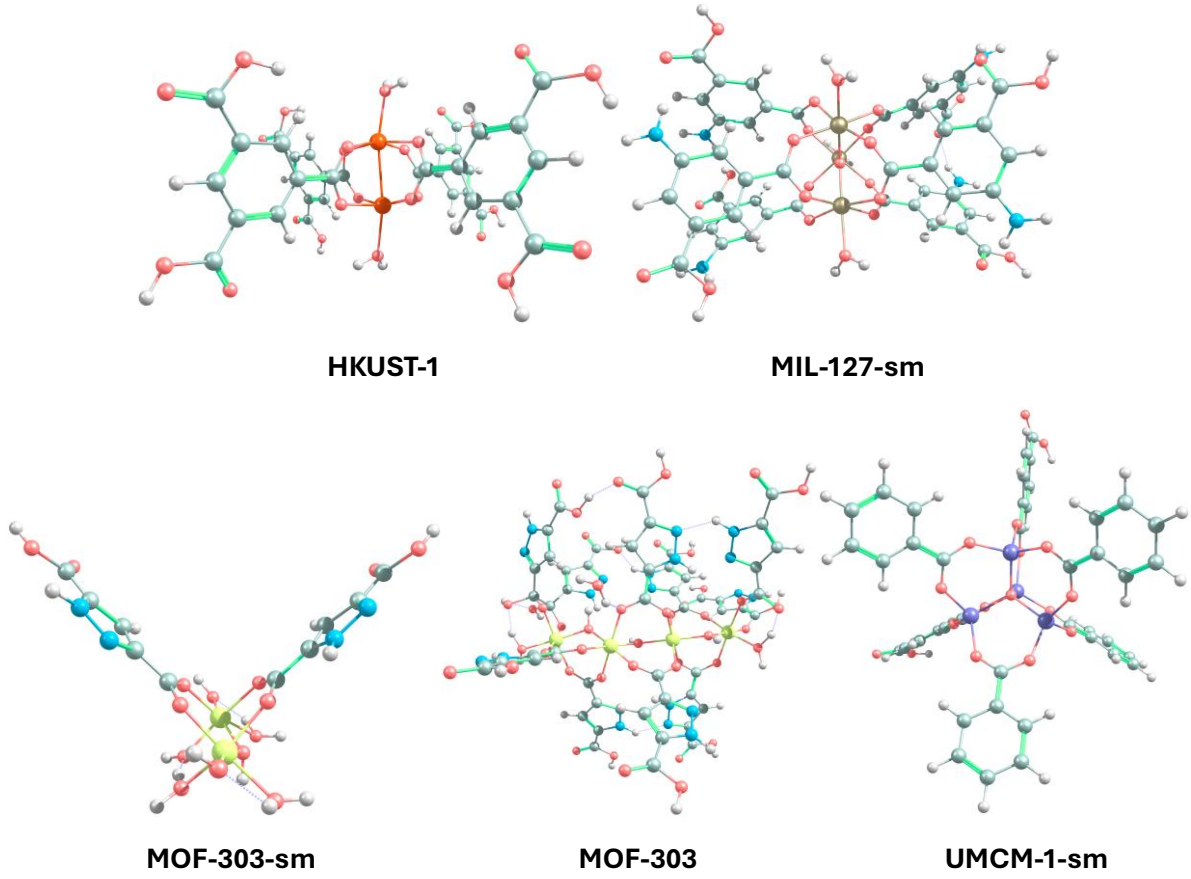

Fig. S3 The MOF models used for reaction path explorations. "sm" in the MOF names indicates that the model is smaller than the ones shown in Fig. 1. The orange, dark yellow, yellow, purple, red, blue, grey and white spheres represent the Cu, Fe, Al, Zn, O, N, C and H atoms, respectively.

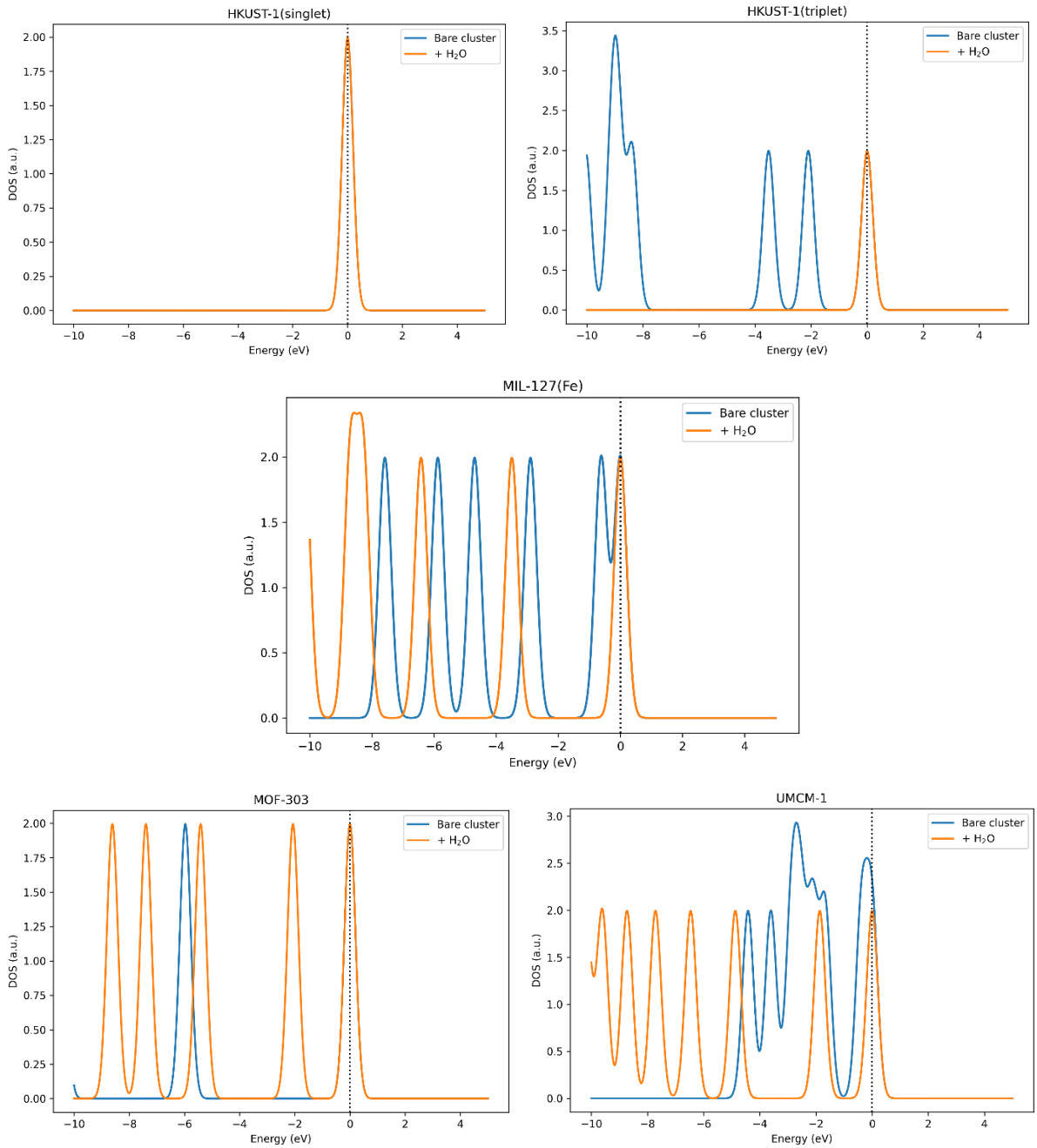

Fig. S4 The density of state (DOS) profiles of the MOF clusters with/without one guest water molecule (Figs. 1 and 2). The dashed vertical line represents the highest occupied molecular orbital (HOMO).

Table S2 The Hirshfeld charges of the HKUST-1(singlet) clusters with n_W = 0 – 10 water molecules obtained from condensation simulations (Fig. S2), at ground state ($q(N)$) and in the presence of an extra electron ($q(N+1)$) (in C), and the corresponding Fukui indices for nucleophilic attack ($f^+ = q(N+1) - q(N)$), reported for atoms with $|f^+| > 0.020$ and the metal ions.

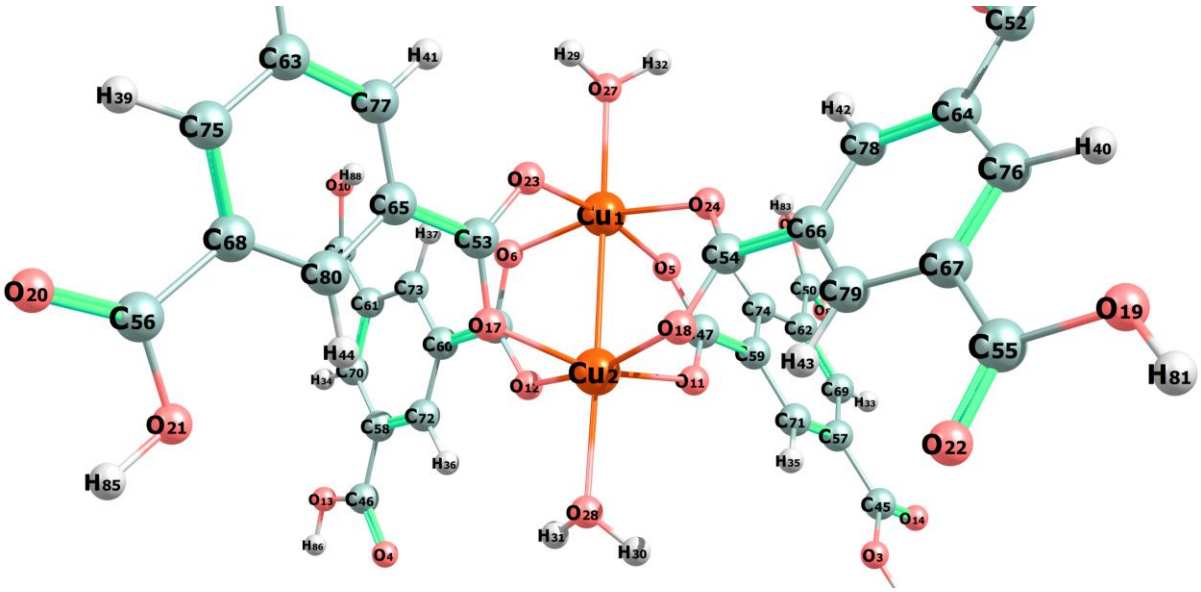

Atom (index)	$q(N)$	$q(N+1)$	f^+	$q(N)$	$q(N+1)$	f^+	$q(N)$	$q(N+1)$	f^+	$q(N)$	$q(N+1)$	f^+
		$n_W = 0$			$n_W = 1$			$n_W = 2$			$n_W = 4$	
Cu1	0.414	0.352	-0.062	0.431	0.397	-0.034	0.445	0.412	-0.033	0.422	0.378	-0.044
Cu2	0.417	0.359	-0.058	0.413	0.350	-0.063	0.460	0.333	-0.126	0.417	0.362	-0.054
O5	-0.253	-0.287	-0.034	-0.248	-0.275	-0.027	-0.262	-0.283	-0.021	-0.250	-0.290	-0.040
O6	-0.252	-0.283	-0.031	-0.246	-0.282	-0.036	-0.245	-0.283	-0.038	-0.249	-0.281	-0.032
O11	-0.256	-0.287	-0.032	-0.266	-0.296	-0.030	-0.256	-0.270	-0.015	-0.261	-0.298	-0.036
O12	-0.254	-0.287	-0.033	-0.257	-0.286	-0.029	-0.262	-0.288	-0.027	-0.247	-0.281	-0.034
O17	-0.246	-0.278	-0.033	-0.247	-0.277	-0.030	-0.239	-0.274	-0.035	-0.243	-0.275	-0.031
O18	-0.249	-0.284	-0.034	-0.247	-0.283	-0.036	-0.252	-0.285	-0.033	-0.245	-0.272	-0.027
O23	-0.258	-0.290	-0.032	-0.247	-0.285	-0.038	-0.237	-0.281	-0.044	-0.237	-0.265	-0.028
O24	-0.257	-0.289	-0.031	-0.260	-0.294	-0.034	-0.265	-0.297	-0.032	-0.241	-0.265	-0.024
C48	0.201	0.180	-0.021	0.201	0.182	-0.019	0.200	0.179	-0.021	0.204	0.185	-0.019
C53	0.200	0.179	-0.021	0.204	0.184	-0.020	0.211	0.187	-0.023	0.204	0.182	-0.022
C54	0.200	0.179	-0.021	0.197	0.174	-0.023	0.195	0.173	-0.022	0.204	0.186	-0.018
Atom (index)	$q(N)$	$q(N+1)$	f^+	$q(N)$	$q(N+1)$	f^+	$q(N)$	$q(N+1)$	f^+			
		$n_W = 6$			$n_W = 8$			$n_W = 10$				
Cu1	0.422	0.308	-0.114	0.428	0.312	-0.116	0.436	0.404	-0.031			
Cu2	0.443	0.445	0.002	0.484	0.452	-0.032	0.416	0.303	-0.113			
O5	-0.243	-0.273	-0.030	-0.303	-0.324	-0.021	-0.215	-0.243	-0.028			
O6	-0.244	-0.280	-0.036	-0.234	-0.253	-0.020	-0.249	-0.293	-0.044			
O11	-0.259	-0.296	-0.037	-0.259	-0.300	-0.041	-0.233	-0.263	-0.030			
O12	-0.242	-0.292	-0.050	-0.237	-0.278	-0.041	-0.249	-0.267	-0.018			
O17	-0.236	-0.274	-0.038	-0.238	-0.281	-0.043	-0.218	-0.241	-0.022			
O18	-0.249	-0.284	-0.035	-0.228	-0.254	-0.026	-0.251	-0.283	-0.032			
O23	-0.241	-0.257	-0.016	-0.241	-0.269	-0.028	-0.232	-0.256	-0.024			
O24	-0.263	-0.266	-0.003	-0.236	-0.248	-0.012	-0.237	-0.277	-0.040			
C48	0.206	0.183	-0.023	0.210	0.191	-0.019	0.200	0.181	-0.018			
C53	0.207	0.185	-0.021	0.210	0.188	-0.023	0.211	0.191	-0.019			
C54	0.198	0.186	-0.012	0.210	0.194	-0.016	0.204	0.182	-0.021			

Table S3 The Hirshfeld charges of the HKUST-1(triplet) clusters with n_W = 0 – 10 water molecules obtained from condensation simulations (Fig. S2), at ground state ($q(N)$) and in the presence of an extra electron ($q(N+1)$) (in C), and the corresponding Fukui indices for nucleophilic attack ($f^+ = q(N+1) - q(N)$), reported for atoms with $|f^+| \geq 0.018$ and the metal ions.

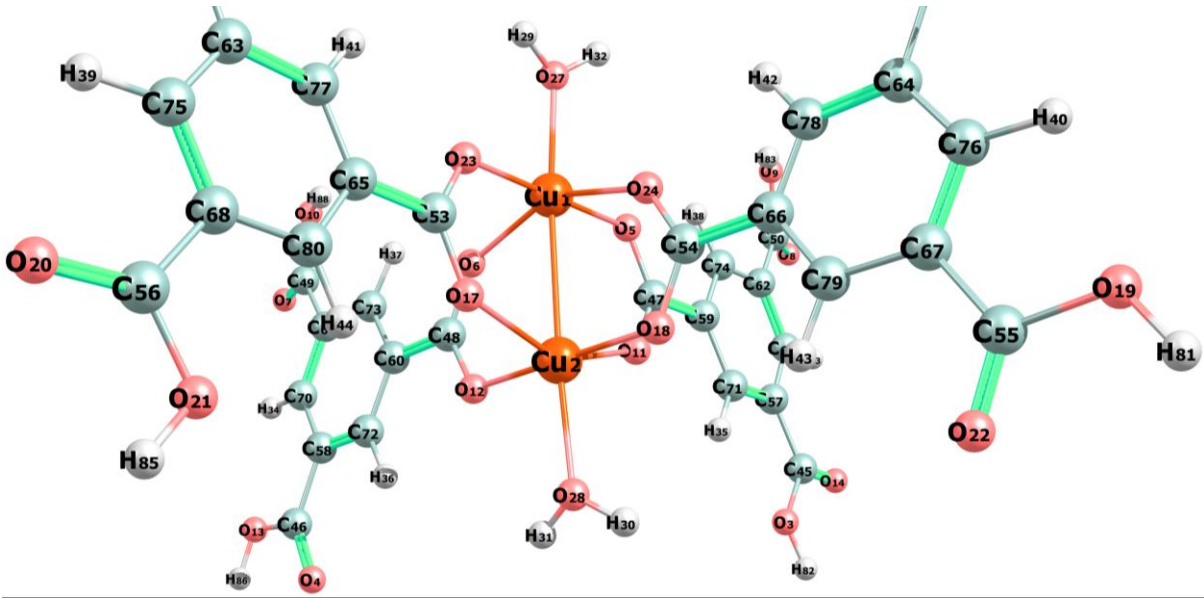

Atom (index)	$q(N)$	$q(N+1)$	f^+	$q(N)$	$q(N+1)$	f^+	$q(N)$	$q(N+1)$	f^+	$q(N)$	$q(N+1)$	f^+
		$n_W = 0$			$n_W = 1$			$n_W = 2$			$n_W = 4$	
Cu1	0.533	0.345	-0.187	0.569	0.360	-0.209	0.566	0.378	-0.188	0.573	0.385	-0.188
Cu2	0.533	0.350	-0.183	0.558	0.367	-0.191	0.553	0.374	-0.179	0.553	0.370	-0.183
O7	-0.257	-0.276	-0.018	-0.255	-0.275	-0.019	-0.257	-0.275	-0.018	-0.257	-0.275	-0.019
O8	-0.255	-0.273	-0.018	-0.242	-0.257	-0.015	-0.296	-0.315	-0.019	-0.253	-0.267	-0.014
O14	-0.276	-0.294	-0.018	-0.281	-0.296	-0.015	-0.274	-0.287	-0.013	-0.283	-0.299	-0.015
O20	-0.285	-0.303	-0.019	-0.282	-0.301	-0.019	-0.283	-0.301	-0.018	-0.282	-0.301	-0.020
C47	0.197	0.178	-0.019	0.192	0.173	-0.019	0.191	0.177	-0.014	0.193	0.175	-0.018
C48	0.200	0.181	-0.020	0.210	0.188	-0.022	0.196	0.178	-0.018	0.209	0.189	-0.021
C53	0.200	0.181	-0.019	0.207	0.186	-0.021	0.209	0.188	-0.020	0.204	0.184	-0.020
C54	0.197	0.178	-0.019	0.201	0.187	-0.014	0.200	0.180	-0.020	0.198	0.186	-0.012
C76	-0.023	-0.042	-0.019	-0.011	-0.024	-0.013	-0.015	-0.034	-0.018	-0.009	-0.021	-0.012

Atom (index)	$q(N)$	$q(N+1)$	f^+	$q(N)$	$q(N+1)$	f^+	$q(N)$	$q(N+1)$	f^+
		$n_W = 6$			$n_W = 8$			$n_W = 10$	
Cu1	0.531	0.340	-0.191	0.556	0.412	-0.145	0.560	0.399	-0.161
Cu2	0.553	0.382	-0.171	0.569	0.373	-0.196	0.574	0.395	-0.179
O7	-0.288	-0.308	-0.020	-0.300	-0.318	-0.019	-0.296	-0.312	-0.016
O8	-0.284	-0.303	-0.018	-0.287	-0.297	-0.010	-0.300	-0.317	-0.018
O14	-0.277	-0.291	-0.014	-0.280	-0.293	-0.013	-0.264	-0.282	-0.018
O20	-0.279	-0.299	-0.019	-0.282	-0.305	-0.022	-0.283	-0.300	-0.017
C47	0.192	0.175	-0.017	0.195	0.184	-0.011	0.207	0.194	-0.013
C48	0.212	0.194	-0.017	0.206	0.187	-0.019	0.198	0.179	-0.019
C53	0.205	0.184	-0.021	0.209	0.189	-0.020	0.219	0.204	-0.015
C54	0.204	0.187	-0.017	0.198	0.184	-0.014	0.204	0.189	-0.015
C76	-0.005	-0.019	-0.014	-0.014	-0.026	-0.013	-0.016	-0.041	-0.025

Table S4 The Hirshfeld charges of the MIL-127(Fe) clusters with $n_W = 0 – 10$ water molecules obtained from condensation simulations (Fig. S1), at ground state ($q(N)$) and in the presence of an extra electron ($q(N+1)$) (in C), and the corresponding Fukui indices for nucleophilic attack ($f^+ = q(N+1) - q(N)$), reported for atoms with $|f^+| \geq 0.012$ and the metal ions.

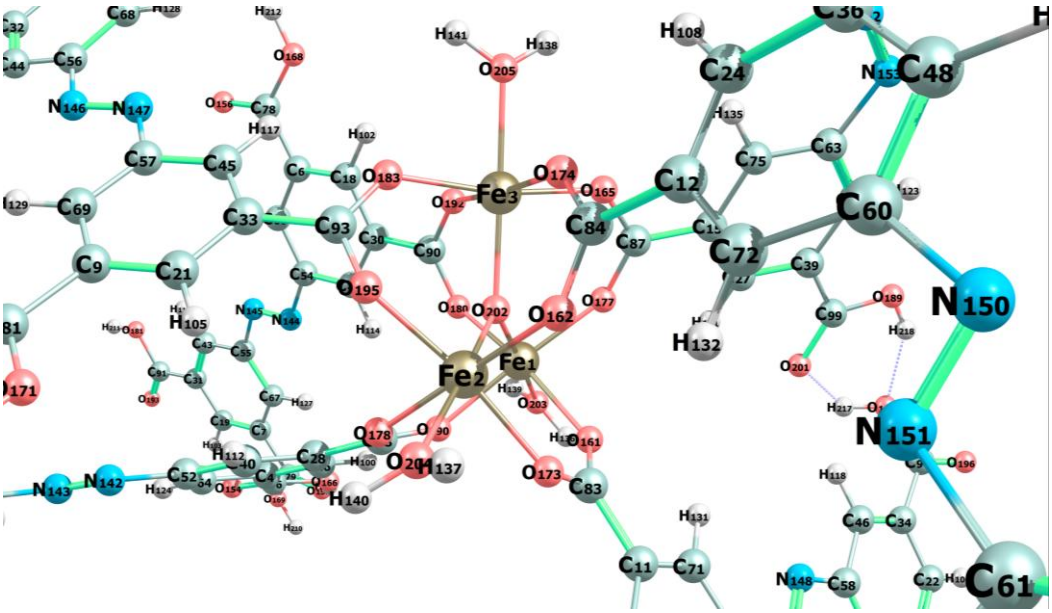

Atom (index)	$q(N)$	$q(N+1)$	f^+	$q(N)$	$q(N+1)$	f^+	$q(N)$	$q(N+1)$	f^+	$q(N)$	$q(N+1)$	f^+
		$n_W = 0$			$n_W = 1$			$n_W = 2$			$n_W = 4$	
Fe1	0.546	0.472	-0.074	0.543	0.439	-0.104	0.545	0.434	-0.111	0.532	0.464	-0.069
Fe2	0.548	0.454	-0.094	0.541	0.410	-0.131	0.540	0.396	-0.144	0.545	0.447	-0.098
Fe3	0.550	0.467	-0.084	0.552	0.517	-0.035	0.551	0.523	-0.027	0.555	0.469	-0.086
C48	-0.020	-0.032	-0.012	-0.009	-0.020	-0.011	-0.010	-0.020	-0.011	-0.025	-0.037	-0.012
C51	0.002	-0.010	-0.012	0.012	0.001	-0.012	0.005	-0.006	-0.012	0.011	0.001	-0.010
C69	-0.003	-0.015	-0.012	-0.001	-0.012	-0.011	-0.001	-0.012	-0.011	-0.004	-0.016	-0.012
C83	0.229	0.213	-0.016	0.228	0.212	-0.016	0.228	0.212	-0.016	0.230	0.213	-0.017
C84	0.233	0.215	-0.018	0.233	0.224	-0.009	0.231	0.224	-0.008	0.228	0.214	-0.014
C87	0.233	0.218	-0.015	0.233	0.220	-0.013	0.232	0.221	-0.011	0.227	0.212	-0.015
C88	0.226	0.212	-0.014	0.229	0.212	-0.017	0.230	0.212	-0.018	0.225	0.211	-0.014
C90	0.229	0.215	-0.014	0.232	0.222	-0.011	0.233	0.223	-0.010	0.232	0.218	-0.014
C93	0.229	0.213	-0.016	0.231	0.219	-0.012	0.231	0.220	-0.011	0.230	0.214	-0.016
O202	-0.373	-0.398	-0.025	-0.375	-0.384	-0.009	-0.375	-0.377	-0.002	-0.380	-0.396	-0.016

Atom (index)	$q(N)$	$q(N+1)$	f^+	$q(N)$	$q(N+1)$	f^+	$q(N)$	$q(N+1)$	f^+
		$n_W = 6$			$n_W = 8$			$n_W = 10$	
Fe1	0.543	0.438	-0.105	0.536	0.427	-0.109	0.548	0.495	-0.053
Fe2	0.544	0.425	-0.119	0.542	0.431	-0.111	0.538	0.420	-0.118
Fe3	0.543	0.503	-0.039	0.542	0.503	-0.040	0.542	0.455	-0.087
C48	-0.031	-0.042	-0.011	-0.030	-0.039	-0.009	-0.030	-0.041	-0.011
C51	0.012	0.001	-0.011	0.000	-0.010	-0.011	0.007	-0.002	-0.009
C69	-0.005	-0.016	-0.011	-0.005	-0.015	-0.010	0.010	-0.002	-0.012
C83	0.231	0.213	-0.018	0.227	0.207	-0.019	0.227	0.212	-0.015
C84	0.231	0.220	-0.010	0.232	0.221	-0.011	0.233	0.217	-0.016
C87	0.226	0.213	-0.013	0.230	0.217	-0.013	0.229	0.220	-0.009
C88	0.229	0.210	-0.018	0.223	0.205	-0.018	0.228	0.215	-0.013
C90	0.231	0.220	-0.011	0.227	0.215	-0.012	0.232	0.220	-0.012
C93	0.231	0.217	-0.014	0.230	0.215	-0.015	0.232	0.213	-0.019
O202	-0.384	-0.395	-0.011	-0.389	-0.402	-0.013	-0.381	-0.399	-0.017

Table S5 The Hirshfeld charges of the MOF-303 clusters with $n_W = 0 – 10$ water molecules obtained from condensation simulations (Fig. S1), at ground state ($q(N)$) and in the presence of an extra electron ($q(N+1)$) (in C), and the corresponding Fukui indices for nucleophilic attack ($f^+ = q(N+1) - q(N)$), reported for atoms with $|f^+| > 0.025$ and the metal ions.

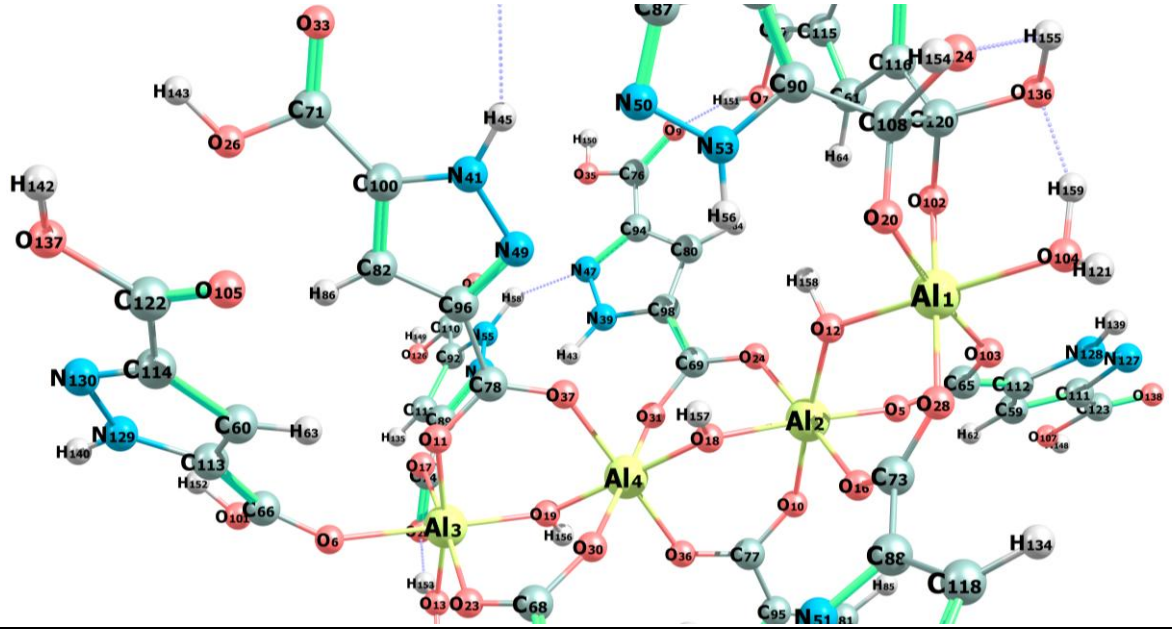

Atom (index)	$q(N)$	$q(N+1)$	f^+	$q(N)$	$q(N+1)$	f^+	$q(N)$	$q(N+1)$	f^+	$q(N)$	$q(N+1)$	f^+
		$n_W = 0$			$n_W = 1$			$n_W = 2$			$n_W = 4$	
Al1	0.394	0.394	0.000	0.398	0.397	-0.001	0.390	0.389	-0.001	0.389	0.388	-0.001
Al2	0.432	0.431	-0.001	0.426	0.424	-0.002	0.432	0.431	-0.001	0.438	0.436	-0.002
Al3	0.442	0.434	-0.008	0.447	0.441	-0.006	0.439	0.434	-0.005	0.436	0.434	-0.002
Al4	0.410	0.409	-0.002	0.412	0.410	-0.002	0.409	0.408	-0.001	0.411	0.411	0.000
O6	-0.165	-0.261	-0.095	-0.166	-0.236	-0.070	-0.147	-0.242	-0.095	-0.263	-0.262	0.001
C60	-0.019	-0.080	-0.061	-0.042	-0.081	-0.039	-0.031	-0.079	-0.049	-0.051	-0.051	0.000
C66	0.263	0.146	-0.117	0.256	0.170	-0.086	0.265	0.155	-0.110	0.216	0.215	-0.001
O101	-0.155	-0.224	-0.070	-0.166	-0.218	-0.052	-0.164	-0.229	-0.065	-0.284	-0.287	-0.003
O105	-0.269	-0.304	-0.035	-0.291	-0.300	-0.009	-0.238	-0.272	-0.035	-0.263	-0.267	-0.003
C113	0.007	-0.026	-0.033	-0.006	-0.023	-0.018	0.010	-0.019	-0.028	0.006	0.007	0.000
C114	0.021	-0.016	-0.037	0.012	-0.011	-0.023	0.011	-0.022	-0.033	-0.005	-0.006	-0.002
N129	0.005	-0.042	-0.047	-0.002	-0.032	-0.030	0.009	-0.035	-0.044	0.014	0.013	-0.001
N130	-0.087	-0.183	-0.096	-0.098	-0.159	-0.061	-0.090	-0.177	-0.087	-0.114	-0.119	-0.005
H140	0.170	0.143	-0.027	0.163	0.146	-0.017	0.172	0.148	-0.024	0.160	0.159	-0.002
H152	0.209	0.177	-0.032	0.204	0.181	-0.024	0.204	0.175	-0.030	0.139	0.136	-0.003

Atom (index)	$q(N)$	$q(N+1)$	f^+	$q(N)$	$q(N+1)$	f^+	$q(N)$	$q(N+1)$	f^+
		$n_W = 6$			$n_W = 8$			$n_W = 10$	
Al1	0.397	0.395	-0.002	0.395	0.394	-0.001	0.401	0.400	-0.002
Al2	0.423	0.421	-0.001	0.428	0.426	-0.002	0.412	0.412	-0.001
Al3	0.434	0.432	-0.003	0.437	0.432	-0.005	0.435	0.433	-0.002
Al4	0.411	0.410	-0.001	0.421	0.418	-0.003	0.402	0.401	-0.001
O6	-0.281	-0.285	-0.004	-0.285	-0.289	-0.004	-0.278	-0.281	-0.004
C60	-0.062	-0.063	-0.001	-0.064	-0.061	0.003	-0.063	-0.064	-0.001
C66	0.204	0.203	-0.001	0.202	0.201	-0.001	0.206	0.204	-0.001
O101	-0.304	-0.307	-0.003	-0.315	-0.319	-0.004	-0.297	-0.300	-0.002
O105	-0.274	-0.279	-0.005	-0.273	-0.271	0.002	-0.275	-0.279	-0.004
C113	0.015	0.013	-0.001	0.014	0.014	0.000	0.014	0.013	-0.001
C114	-0.010	-0.011	-0.001	-0.008	-0.009	-0.001	-0.010	-0.011	-0.001
N129	0.018	0.020	0.002	0.018	0.016	-0.001	0.018	0.019	0.001
N130	-0.124	-0.121	0.003	-0.122	-0.128	-0.005	-0.124	-0.122	0.002
H140	0.163	0.162	0.000	0.168	0.165	-0.003	0.163	0.163	0.000
H152	0.143	0.141	-0.002	0.161	0.159	-0.002	0.139	0.137	-0.001

Table S6 The Hirshfeld charges of the UMCM-1 clusters with $n_W = 0 – 10$ water molecules obtained from condensation simulations (Fig. S1), at ground state ($q(N)$) and in the presence of an extra electron ($q(N+1)$) (in C), and the corresponding Fukui indices for nucleophilic attack ($f^+ = q(N+1) - q(N)$), reported for atoms with $|f^+| \geq 0.013$ and the metal ions.

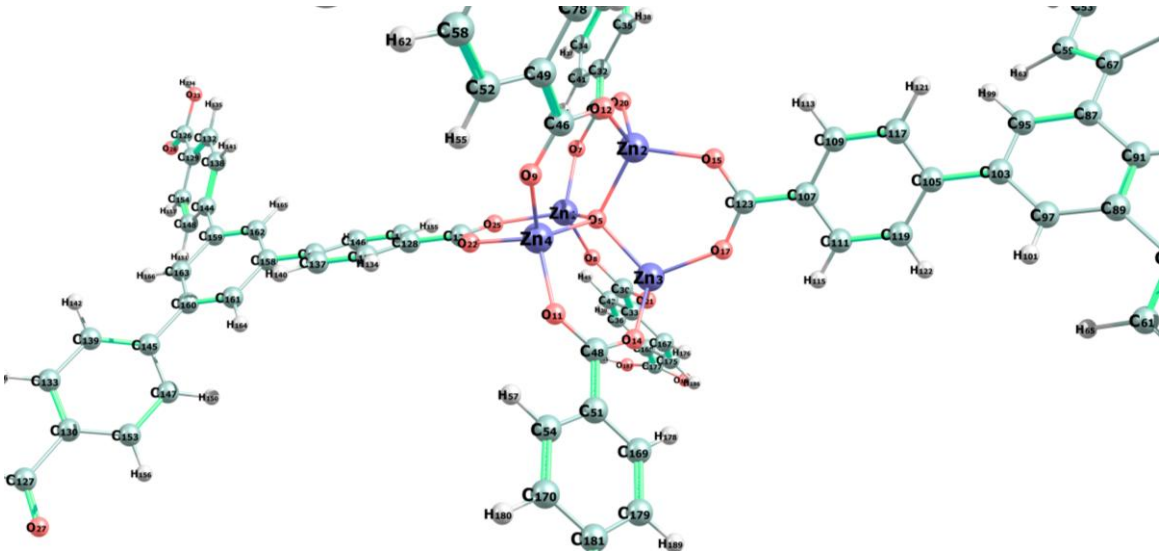

Atom (index)	$q(N)$	$q(N+1)$ $n_W = 0$	f^+	$q(N)$	$q(N+1)$ $n_W = 1$	f^+	$q(N)$	$q(N+1)$ $n_W = 2$	f^+	$q(N)$	$q(N+1)$ $n_W = 4$	f^+
Zn1	0.482	0.476	-0.005	0.482	0.477	-0.005	0.475	0.470	-0.004	0.463	0.458	-0.005
Zn2	0.482	0.479	-0.004	0.472	0.467	-0.004	0.483	0.478	-0.005	0.461	0.457	-0.004
Zn3	0.483	0.479	-0.004	0.477	0.474	-0.003	0.459	0.457	-0.002	0.460	0.457	-0.002
Zn4	0.482	0.481	-0.002	0.485	0.481	-0.005	0.460	0.458	-0.002	0.458	0.456	-0.002
O6	-0.258	-0.281	-0.023	-0.246	-0.277	-0.031	-0.208	-0.244	-0.036	-0.203	-0.248	-0.045
O8	-0.260	-0.270	-0.010	-0.262	-0.266	-0.004	-0.263	-0.266	-0.003	-0.259	-0.276	-0.016
O13	-0.264	-0.276	-0.013	-0.270	-0.276	-0.007	-0.268	-0.276	-0.008	-0.278	-0.290	-0.013
O19	-0.201	-0.214	-0.013	-0.184	-0.201	-0.017	-0.175	-0.201	-0.025	-0.170	-0.197	-0.027
O20	-0.258	-0.271	-0.013	-0.275	-0.286	-0.012	-0.270	-0.285	-0.015	-0.265	-0.287	-0.022
C28	0.209	0.195	-0.013	0.216	0.194	-0.022	0.231	0.197	-0.034	0.231	0.191	-0.040
C29	0.213	0.197	-0.017	0.205	0.189	-0.016	0.206	0.190	-0.015	0.198	0.178	-0.021
C30	0.213	0.198	-0.016	0.211	0.203	-0.008	0.209	0.200	-0.009	0.205	0.186	-0.018
C31	-0.013	-0.030	-0.017	-0.018	-0.037	-0.019	-0.026	-0.045	-0.019	-0.018	-0.046	-0.028
C40	-0.024	-0.036	-0.013	-0.023	-0.039	-0.015	-0.028	-0.048	-0.020	-0.023	-0.050	-0.027
O188	-0.258	-0.280	-0.022	-0.259	-0.275	-0.016	-0.265	-0.282	-0.017	-0.244	-0.277	-0.034

Atom (index)	$q(N)$	$q(N+1)$ $n_W = 6$	f^+	$q(N)$	$q(N+1)$ $n_W = 8$	f^+	$q(N)$	$q(N+1)$ $n_W = 10$	f^+
Zn1	0.472	0.470	-0.002	0.472	0.468	-0.004	0.459	0.457	-0.002
Zn2	0.470	0.468	-0.002	0.460	0.459	-0.002	0.456	0.455	-0.001
Zn3	0.461	0.456	-0.005	0.475	0.473	-0.002	0.465	0.463	-0.002
Zn4	0.449	0.447	-0.002	0.456	0.454	-0.002	0.449	0.448	-0.001
O6	-0.278	-0.285	-0.007	-0.259	-0.278	-0.019	-0.260	-0.276	-0.017
O8	-0.260	-0.273	-0.013	-0.243	-0.257	-0.013	-0.263	-0.269	-0.006
O13	-0.271	-0.275	-0.004	-0.265	-0.270	-0.005	-0.264	-0.271	-0.007
O19	-0.222	-0.224	-0.002	-0.203	-0.212	-0.009	-0.201	-0.211	-0.010
O20	-0.268	-0.271	-0.003	-0.239	-0.248	-0.009	-0.250	-0.257	-0.007
C28	0.205	0.204	-0.001	0.208	0.198	-0.010	0.208	0.198	-0.010
C29	0.209	0.208	-0.001	0.208	0.198	-0.010	0.208	0.199	-0.008
C30	0.213	0.190	-0.023	0.217	0.196	-0.021	0.206	0.197	-0.008
C31	-0.009	-0.013	-0.004	-0.015	-0.027	-0.012	-0.016	-0.028	-0.012
C40	-0.033	-0.037	-0.004	-0.022	-0.032	-0.010	-0.025	-0.033	-0.008
O188	-0.256	-0.284	-0.029	-0.238	-0.267	-0.028	-0.257	-0.274	-0.017

Table S7 Changes in the relative electronic energies ($\Delta E_r = E_{triplet} - E_{singlet}$) and Gibbs free energies ($\Delta G_r = G_{triplet} - G_{singlet}$) of the triplet and singlet HKUST-1 models (kJ mol^{-1}) and their Cu-Cu bond lengths ($L_{Cu\text{-}Cu}$) (Å) with the number of guest water molecules (n_W = 0 – 16).

n_W	ΔE_r	ΔG_r	$L_{Cu\text{-}Cu}$ (singlet)	$L_{Cu\text{-}Cu}$ (triplet)	S^2A^a (triplet)
0	-163.6	-167.9	2.72	2.89	2.00
1	-215.8	-200.2	2.77	3.18	2.00
2	-138.4	-148.1	2.86	3.17	2.00
4	-233.1	-214.8	2.75	3.20	2.00
6	-138.8	-143.6	2.91	2.97	2.00
8	-215.3	-230.4	3.06	3.23	2.00
10	-167.8	-162.8	2.85	3.24	2.00
12	-264.8	-265.2	2.78	3.09	2.00
16	-177.1	-184.2	2.95	3.46	2.00

[a] Total spin eigenvalue.

Table S8 Changes in the APT atomic charges of the Cu atoms (C_{Cu}) (C) and the longest Cu-Oc bond lengths ($L_{Cu\text{-}Oc}$) (Å) of the neutral triplet HKUST-1 model and the doublet HKUST-1 state (with -1 charge) with the number of guest water molecules (n_W = 0 – 6).

n_W	$L_{Cu\text{-}Oc,triplet}$	$L_{Cu\text{-}Oc,doublet}$	$C_{Cu1,triplet}$	$C_{Cu2,triplet}$	$C_{Cu1,doublet}$	$C_{Cu2,doublet}$
0	2.07	4.36*	1.74	1.75	0.64	1.69
1	2.84*	3.52*	1.55	1.71	0.72	1.61
2	2.59**	2.94*	1.62	1.70	0.75	1.50
6	2.17**	3.12*	1.64	1.70	0.72	1.60

* Structures with detached carboxylate groups.

** Structures with elongated Cu-Oc bonds.

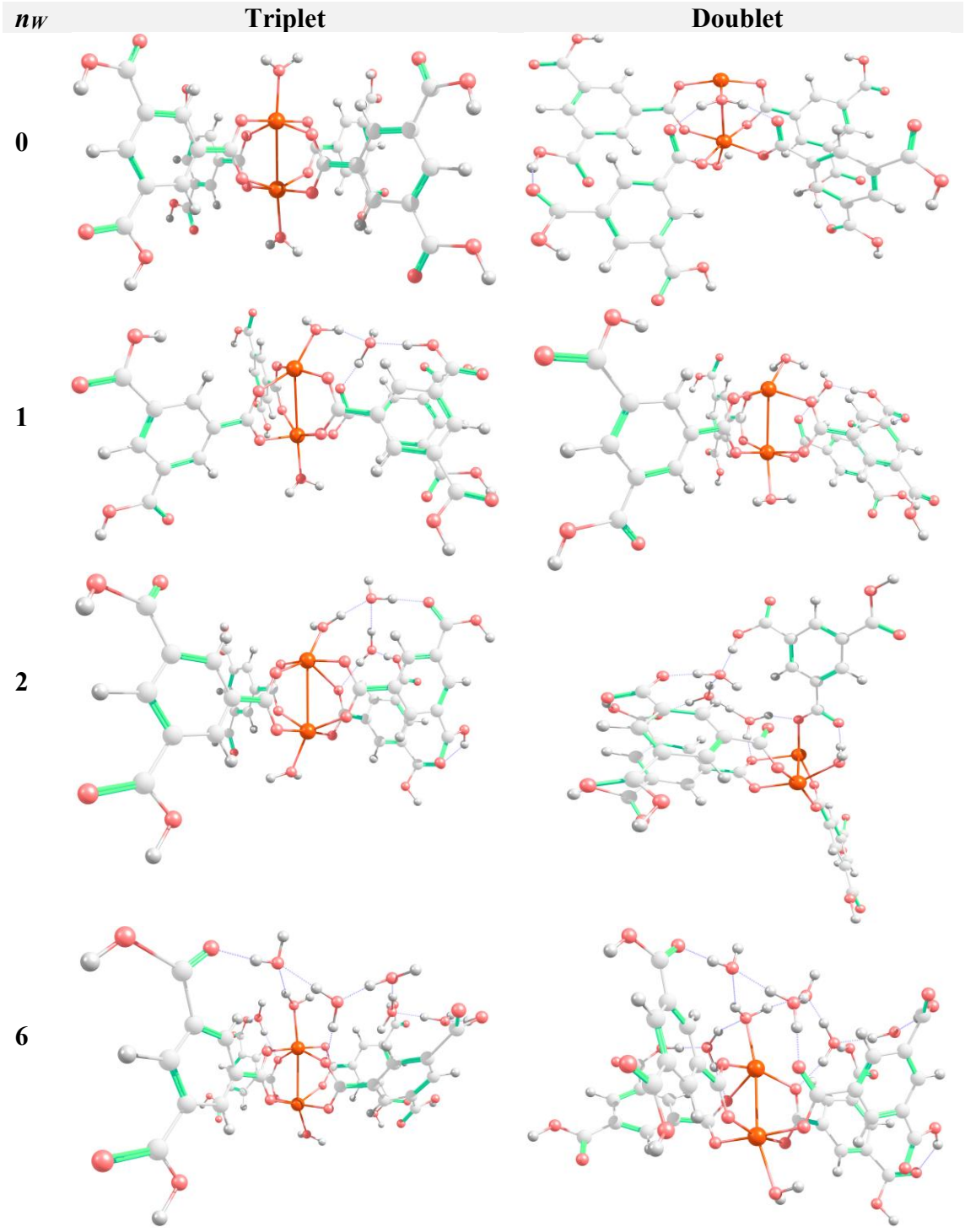

Fig. S5 Changes in the structure of triplet and doublet HKUST-1 induced by n_W = 0, 1, 2 and 6 guest water molecules. The Cu, O, C and H atoms are represented by orange, red, light grey and white spheres, respectively. The dotted blue lines show hydrogen bonds.

References

1 J. Bae, S. H. Park, D. Moon and N. C. Jeong, *Commun. Chem.*, 2022, **5**, 51.

2 N. Hanikel, X. Pei, S. Chheda, H. Lyu, W. Jeong, J. Sauer, L. Gagliardi and O. M. Yaghi, *Science*, 2021, **374**, 545.

3 K. Koh, A. G. Wong-Foy and A. J. Matzger, *Angew. Chem., Int. Ed.*, 2008, **47**, 677.

4 C. R. Groom, I. J. Bruno, M. P. Lightfoot and S. C. Ward, *Acta Crystallogr., Sect. B*, 2016, **72**, 171–179.

5 Y. Belmabkhout, R. S. Pillai, D. Alezi, O. Shekhah, P. M. Bhatt, Z. Chen, K. Adil, S. Vaesen, G. De Weireld, M. Pang, M. Suetin, A. J. Cairns, V. Solovyeva, A. Shkurenko, O. El Tall, G. Maurin and M. Eddaoudi, *J. Mater. Chem. A*, 2017, **5**, 3293.

6 F. Keshavarz, *Chem. Mater.*, 2023, **36**, 439–449.

7 G. Kresse and J. Furthmüller, *Comput. Mater. Sci.*, 1996, **6**, 15–50.

8 G. Kresse and J. Furthmüller, *Phys. Rev. B*, 1996, **54**, 11169.

9 J. Sun, A. Ruzsinszky and J. P. Perdew, *Phys. Rev. Lett.*, 2015, **115**, 036402.

10 J. Sun, R. C. Remsing, Y. Zhang, Z. Sun, A. Ruzsinszky, H. Peng, Z. Yang, A. Paul, U. Waghmare, X. Wu, M. L. Klein and J. P. Perdew, *Nat. Chem.*, 2016, **8**, 831–836.

11 G. Kresse and D. Joubert, *Phys. Rev. B*, 1999, **59**, 1758.

12 S. Grimme, J. Antony, S. Ehrlich and H. Krieg, *J. Chem. Phys.*, 2010, **132**, 154104.

13 S. Grimme, S. Ehrlich and L. Goerigk, *J. Comput. Chem.*, 2011, **32**, 1456–1465.

14 D. M. Bylander, L. Kleinman and S. Lee, *Phys. Rev. B*, 1990, **42**, 1394.

15 M. J. Frisch, G. W. Trucks, H. B. Schlegel, G. E. Scuseria, M. A. Robb, J. R. Cheeseman, G. Scalmani, V. Barone, G. A. Petersson, H. Nakatsuji, X. Li, M. Caricato, A. V. Marenich, J. Bloino, B. G. Janesko, R. Gomperts, B. Mennucci, et al., *Gaussian 16, Revision C.02; Gaussian, Inc.: Wallingford CT*, 2019.

16 J. Heyd, G. E. Scuseria and M. Ernzerhof, *J. Chem. Phys.*, 2003, **118**, 8207–8215.

17 C. Adamo and V. Barone, *J. Chem. Phys.*, 1999, **110**, 6158–6170.

18 T. H. Dunning Jr. and P. J. Hay, In *Modern Theoretical Chemistry*; H. F. Schaefer III, Ed.; Plenum: New York, 1977; Vol. 3, pp. 1–28.

19 W. R. Wadt and P. J. Hay, *J. Chem. Phys.*, 1985, **82**, 284–298.

20 Y. Zhao and D. G. Truhlar, *Theor. Chem. Acc.*, 2008, **120**, 215–241.

21 G. A. Zhurko, *Chemcraft—graphical program for visualization of quantum chemistry computations*, Ivanovo, Russia, 2005. Available at: https://chemcraftprog.com.

22 D. C. Young, *Computational Chemistry: A Practical Guide for Applying Techniques to Real World Problems*; Wiley: New York, 2001.

23 M. K. Agusta, A. G. Saputro, V. V. Tanuwijaya, N. N. Hidayat and H. K. Dipojono, *Procedia Eng.*, 2017, **170**, 136–140.

24 M. Todaro, G. Buscarino, L. Sciortino, A. Alessi, F. Messina, M. Taddei, M. Ranocchiari, M. Cannas and F. M. Gelardi, *J. Phys. Chem. C*, 2016, **120**, 12879–12889.

25 W. Xue, Z. Zhang, H. Huang, C. Zhong and D. Mei, *J. Phys. Chem. C*, 2019, **124**, 1991–2001.

26 C. Peng, P. Y. Ayala, H. B. Schlegel and M. J. Frisch, *J. Comput. Chem.*, 1996, **17**, 49–56.

27 K. Fukui, *Acc. Chem. Res.*, 1981, **14**, 363–368.

28 H. P. Hratchian and H. B. Schlegel, In *Theory and Applications of Computational Chemistry: The First 40 Years*; C. E. Dykstra, G. Frenking, K. S. Kim and G. Scuseria, Eds.; Elsevier: Amsterdam, 2005; pp. 195–249.

29 J. Kubecka, V. Besel, T. Kurtén, N. Myllys and H. Vehkamäki, *J. Phys. Chem. A*, 2019, **123**, 6022–6033.

30 J. Zhang and M. Dolg, *Phys. Chem. Chem. Phys.*, 2015, **17**, 24173–24181.

31 J. Zhang and M. Dolg, *Phys. Chem. Chem. Phys.*, 2016, **18**, 3003–3010.

32 D. E. Coupry, M. A. Addicoat and T. Heine, *J. Chem. Theory Comput.*, 2016, **12**, 5215–5225.

33 C. Bannwarth, S. Ehlert and S. Grimme, *J. Chem. Theory Comput.*, 2019, **15**, 1652–1671.

34 S. Grimme, C. Bannwarth and P. Shushkov, *J. Chem. Theory Comput.*, 2017, **13**, 1989–2009.